A general SER formula for an OFDM system with MDPSK in frequency domain over Rayleigh fading channels

A General SER Formula for an OFDM System With MDPSK in Frequency Domain Over Rayleigh Fading Channels

Kun Zhong, Tjeng Thiang Tjhung, *Senior Member, IEEE*, and Fumiyuki Adachi, *Fellow, IEEE*

***Abstract*—A closed-form formula for symbol-error rate (SER) of an orthogonal frequency-division multiplexing (OFDM) system with M-ary differential phase-shift keying (MDPSK) in frequency domain over Rayleigh fading channels is obtained. It is found that, by MDPSK in frequency domain, identical SERs can be achieved on all subcarriers. However, both time and frequency dispersion in the channel will introduce error floors. A comparison between OFDM-MDPSK in frequency domain and that in time domain reveals that the former system offers superior SER performance in a fast fading environment, while the latter performs better if the channel is mainly frequency selective. Moreover, the former system has lower implementation complexity.**

***Index Terms*—Guard interval, M-ary differential phase-shift keying (MDPSK), orthogonal frequency-division multiplexing (OFDM), Rayleigh fading, symbol-error rate (SER).**

I. Introduction

THE POPULARITY of orthogonal frequency-division multiplexing (OFDM) systems is rising due to its ability to support high-data-rate transmission over time-variant multipath fading channels. OFDM transmission techniques have found applications in the two digital terrestrial broadcasting services—digital audio broadcasting (DAB) and digital terrestrial video broadcasting (DTVB) [1], [2]. OFDM is used in the standards for wireless 5-GHz local area networks (IEEE 802.11a in US and HIPERLAN in Europe) [3], [4]. Asymmetric digital subscriber lines (ADSL) based on OFDM technology are used to deliver high-rate digital data over existing plain old telephone lines (pots) [5]. OFDM can also serve as an alternative transmission method to digital european cordless telephone (DECT)-like digital cordless systems [6].

In OFDM, we simultaneously transmit a block of data symbols on a group of subcarriers with frequency-division multiplexing. Within one OFDM symbol duration, each subcarrier is modulated with a data symbol using any conventional method, such as quadrature amplitude modulation (QAM), M-ary phase-shift keying (MPSK), M-ary differential phase-shift keying (MDPSK), as in a single-carrier system. The spacing between adjacent subcarriers is carefully selected so that each subcarrier is located on all the others' spectral nulls, and all the subcarriers are also packed as closely as possible. Because of this spectral orthogonality, the modulation symbols on all the subcarriers can be ideally recovered by sampling the received baseband signal at a rate which is the reciprocal of the intercarrier spacing followed by a fast Fourier transform (FFT). In this paper, we consider the case that, during the transmission of one block of data, the modulation symbols on all the subcarriers are formed by sequentially MDPSK-modulating the data symbols from the current block; this is called OFDM with differential encoding in *frequency* domain. Instead, we can also MDPSK-modulate the same subcarrier with symbols from contiguous data blocks. However, this latter MDPSK subcarrier modulation technique is called OFDM with differential encoding in *time* domain.

In the next section, the system model for the OFDM-MDPSK in frequency domain is described and compared with that for the OFDM-MDPSK in time domain. This is followed by a specification of the Rayleigh fading channel models used in this paper. Then Adachi and Tjhung's formula [7] is re-examined, where we explicitly show the relationship between the normalized correlation coefficient and the functional behavior of the cumulative distribution function (cdf) of the differential phase angle between two Rayleigh vectors perturbed by Gaussian noise. Next, this cdf is used to evaluate symbol-error rate (SER) performance of the OFDM system over Rayleigh fading channels with various delay and Doppler shift characteristics. A comparison on error performance is also done between OFDM-MDPSK in frequency domain and that in time domain.

II. System Model

The baseband system model for OFDM-MDPSK in frequency domain is shown in Fig. 1(a). The input to the system (at point a in the figure) are bits with a bit rate of R_b. The symbol generator takes $\log_2 M$ consecutive bits at a time and generates one data symbol $\theta_{j,k}$ according to Gray code mapping; N consecutive data symbols form one data block. The indexes j and k are, respectively, the time index (jth data block) and the frequency index (kth subcarrier). The data symbol $\theta_{j,k}$ is allowed any one of the values of $2\pi m/M$ ($m = 0, 1, \ldots, M-1$). At the beginning of the jth data block, the MDPSK modulator sets

Paper approved by C. Tellambura, the Editor for Modulation and Signal Design of the IEEE Communications Society. Manuscript received October 16, 2001; revised June 18, 2002; July 17, 2003; and August 15, 2003.

K. Zhong was with the Department of Electrical and Computer Engineering, National University of Singapore, Singapore 119260. He is now with the Centre for Communications Systems, DSO National Laboratories, Singapore 118230 (e-mail: zkun@dso.org.sg).

T. T. Tjhung is with the Institute for Infocomm Research, Agency for Science, Technology, and Research, Singapore 119613 (e-mail: tjhungtt@i2r.a-star.edu.sg).

F. Adachi is with the Electrical and Communication Engineering Department, Graduate School of Engineering, Tohoku University, Sendai 980-8579, Japan (e-mail: adachi@ecei.tohoku.ac.jp).

Digital Object Identifier 10.1109/TCOMM.2004.826342

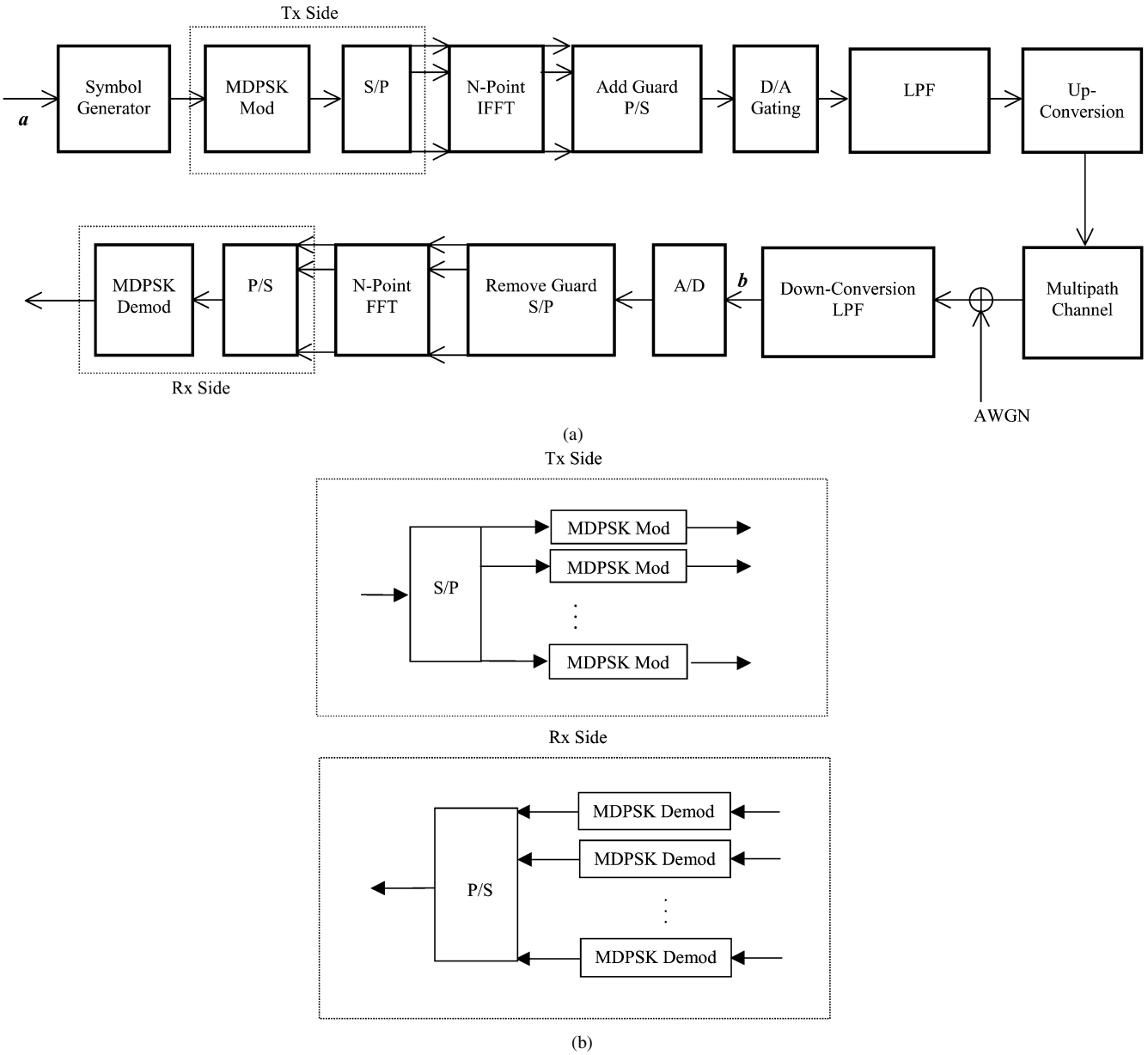

Fig. 1. (a). System model of the uncoded OFDM-MDPSK in frequency domain. (b) Parts of system model for OFDM-MDPSK in time domain which are different from the corresponding parts of OFDM-MDPSK in frequency domain.

$C_{j,-1} = 1$. At the output of the modulator, the kth modulation symbol in the jth data block can be expressed as

$$C_{j,k} = C_{j,k-1} \cdot \exp(\mathrm{i}\theta_{j,k})(k = 0, 1, \ldots, N-1; \mathrm{i} = \sqrt{-1}) \tag{1}$$

After the serial-to-parallel (S/P) conversion, the N modulation symbols in one data block are in parallel at the input of the N-point inverse fast Fourier transform (IFFT) processor. The N post-IFFT samples of this data block, again in parallel, can be written as $c_{j,k'} = (1/\sqrt{N}) \sum_{k=0}^{N-1} C_{j,k} \cdot \exp(\mathrm{i}2\pi kk'/N)(k' = 0, 1, \ldots, N-1)$, where the indexes j and k have the same connotations as mentioned before, and the index k' indicates the position of the complex-valued sample $c_{j,k'}$ in the jth post-IFFT block. To reduce the effect of intersymbol interference (ISI) due to channel multipath, a cyclic prefix of N_g samples is inserted before the N post-IFFT samples, such that $c^g_{j,k'} = c_{j,k'+N}$ $(k' = -N_g, \ldots, -1)$ and $c^g_{j,k'} = c_{j,k'}$ $(k' = 0, \ldots, N-1)$. Now every post-IFFT block contains $N + N_g$ samples. The addition of the cyclic prefix is followed by a parallel-to-serial (P/S) conversion, and the output is a discrete-time sequence. Suppose every post-IFFT block has a duration of T, the sampling period T_s (i.e., the spacing between adjacent samples in the discrete-time sequence) is equal to $T/(N + N_g)$. The useful period in one block has a duration of $T_u = NT_s = NT/(N + N_g)$ and the guard interval $T_g = N_gT_s = N_gT/(N+N_g)$. After digital-to-analog (D/A) conversion, windowing operation, and amplification, the baseband transmitted OFDM signal waveform at the output of the lowpass filter can be represented in a complex form as

$$s(t) = \sum_{j=-\infty}^{+\infty} p(t - jT)\sqrt{P_0} \sum_{k=0}^{N-1} C_{j,k} \cdot \exp[\mathrm{i}\omega_0 k(t - jT)] \tag{2}$$

where $P_0 = E_0/NT_s$ (E_0 is the energy of any one of the complex-valued exponential signals in (2) over one useful period), and $\omega_0 = 2\pi/NT_s$. The windowing function $p(t)$ is assumed to be a unit rectangular pulse defined on the time interval $(-N_gT_s, NT_s)$. In this paper, we assume that N is sufficiently large and the bandwidth of the OFDM signal is approximately $1/T_s$. The lowpass filter is assumed to have an ideal bandwidth of $1/T_s$ to match that of the OFDM signal.

The channel is modeled as a wide-sense stationary uncorrelated scattering (WSSUS) Rayleigh fading channel. At the receiver, we assume ideal down-conversion and lowpass filtering, as well as perfect OFDM symbol synchronization. The analog-to-digital (A/D) converter samples the baseband received waveform $u(t)$ at a sampling rate of $f_s = 1/T_s$. The Remove Guard and S/P unit takes a block of $N + N_g$ consecutive samples, removes the leading N_g samples, and parallels the remaining N samples. The N post-FFT symbols [denoted as $Y_{j,k}$ $(k = 0, 1, \ldots, N-1)$] form one data block. After the P/S conversion, each pair of adjacent symbols in the jth block are compared at the MDPSK demodulator to make the estimation of $\theta_{j,k}$, which is

$$\begin{aligned}\hat{\theta}_{j,k} = {} & \text{the data symbol associated with} \\ & \text{the decision region where} \\ & \arg(Y^*_{j,k-1} \cdot Y_{j,k})\ (k = 0, 1, \ldots, N-1) \text{ falls} \end{aligned} \quad (3)$$

where $Y_{j,-1} = \sqrt{P_0}$ by default.

In contrast, for OFDM system with MDPSK in the time domain, the devices enclosed in the two dashed boxes in Fig. 1(a) have a different sequence of arrangement, as illustrated in Fig. 1(b). As evident from Fig. 1(b), OFDM-MDPSK in frequency domain has a much lower system complexity than its time-domain counterpart, as the latter requires one modulator-demodulator pair for each subcarrier.

III. Channel Model

The channels considered in this paper are WSSUS Rayleigh fading channels with distinct multipath delays. Let us express the received baseband waveform as

$$u(t) = \sum_l h_l(t) s(t - \tau_l) \quad (4)$$

where $h_l(t)$ is the channel impulse response of the lth multipath, τ_l the associated delay, and $s(t)$ the transmitted baseband waveform as defined in (2). Each $h_l(t)$ is modeled as a zero-mean complex-valued Gaussian process with mean power $\sigma^2_{h_l}$ with $\sigma^2_{h_0} + \sigma^2_{h_1} + \sigma^2_{h_2} + \ldots = 1$. Since the channel is assumed to be WSSUS, we have

$$\begin{aligned}\mathrm{E}[h^*_m(t_1) \cdot h_n(t_2)] &= \mathrm{E}[h^*_m(t_1)] \cdot \mathrm{E}[h_n(t_2)] \\ &= 0 \quad (m \neq n). \end{aligned} \quad (5)$$

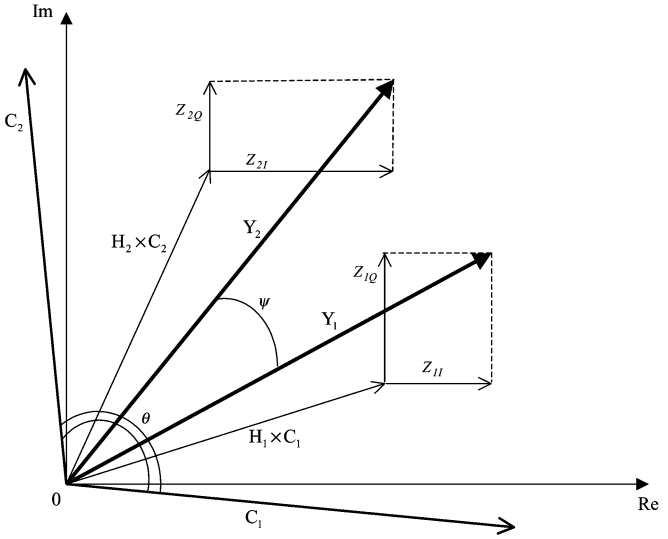

Fig. 2. Geometry for angle between Rayleigh-faded signal vectors perturbed by Gaussian noise.

If we follow Clarke's model [8], [9], the self-correlation on the lth multipath is given by

$$\begin{aligned}\mathrm{R}_{h_l}(t_1, t_2) &= \frac{1}{2}\mathrm{E}[h^*_l(t_1) \cdot h_l(t_2)] \\ &= \sigma^2_{h_l} \mathrm{J}_0[2\pi f_D(t_2 - t_1)] \end{aligned} \quad (6)$$

where $\mathrm{J}_0(\cdot)$ is the zeroth-order Bessel function of the first kind and f_D is the maximum Doppler shift.

Only one-sided exponential power delay profile will be considered in this paper, since it is a generalization of the uniform profile and double-spike profile, both of which are also analyzed in [10]. The exponential profile is given by

$$\sigma^2_{h_l} = \exp(-\alpha\tau_l) \Big/ \sum_{l=0}^{L-1} \exp(-\alpha\tau_l) \ \ (l = 0, 1, \ldots, L-1) \quad (7)$$

where α is a positive attenuation factor, and L the total number of distinct delays.

IV. Distribution of Phase Angle Between Two Rayleigh Vectors Perturbed by Gaussian Noise

Consider the geometry as illustrated in Fig. 2, which reflects a Rayleigh fading communications scenario. Here the two transmitted signal vectors, C_1 and C_2, are of equal amplitude in the complex plane. They are perturbed, first by two multiplicative fading terms, H_1 and H_2, both of which are complex-valued zero-mean Gaussian random variables. The resultant vectors (complex numbers) are $H_1 \times C_1$ and $H_2 \times C_2$, and they are further disturbed by additive complex-valued zero-mean Gaussian noise, Z_1 and Z_2, respectively. As indicated in the figure, the in-phase and quadrature components of Z_1 and Z_2 are $Z_{1\mathrm{I}}$ and $Z_{2\mathrm{I}}, Z_{1\mathrm{Q}}$ and $Z_{2\mathrm{Q}}$, respectively. The received vectors are denoted as Y_1 and $Y_2 (Y_{1,2} = H_{1,2} \times C_{1,2} + Z_{1,2})$, and the angle between them $\psi = \angle Y_2 - \angle Y_1$. The phase angle between the two transmitted signal vectors, C_1 and C_2, is represented by $\theta = \angle C_2 - \angle C_1$. Let $\Delta\eta = \theta - \psi$, then the cdf of the differen-

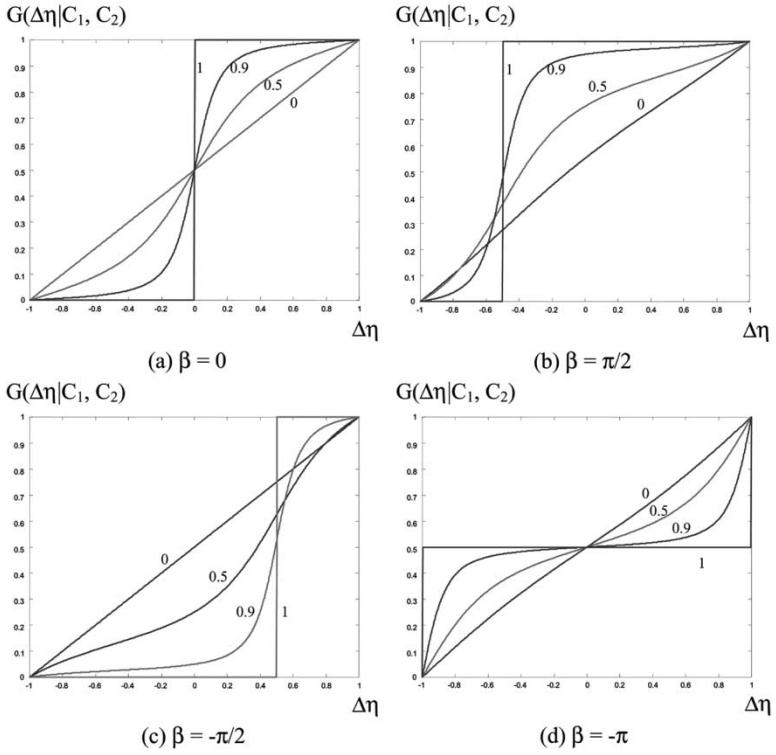

Fig. 3. Illustration of the functional behavior of the conditional cdf $\mathrm{G}(\Delta\eta \mid \mathrm{C}_1, \mathrm{C}_2)$ at various values of $\sqrt{\mathrm{r}^2+\lambda^2}$ and β. The horizontal $\Delta\eta$ axis is normalized with respect to π, so that $\Delta\eta$ lies within the interval $(-1, 1)$. The numbers beside the curves in each of the four subplots indicate the values of $\sqrt{\mathrm{r}^2+\lambda^2}$ for the corresponding curves.

tial phase $\Delta\eta$ conditioned on the two transmitted signal vectors C_1 and C_2 is given by [7]

$$\begin{aligned}\mathrm{G}(\Delta\eta \,|\, C_1, C_2) = \frac{1}{2}\Bigg\{1 + \frac{\Delta\eta}{\pi} - \frac{1}{\pi} \\ \cdot \frac{\sqrt{r^2+\lambda^2}\sin(-\Delta\eta-\beta)}{\sqrt{1-(r^2+\lambda^2)\cos^2(-\Delta\eta-\beta)}} \\ \times \left[\frac{\pi}{2} + k_1\right] + \frac{1}{\pi}\cdot\frac{\sqrt{r^2+\lambda^2}\sin\beta}{\sqrt{1-(r^2+\lambda^2)\cos^2\beta}} \\ \times \left[\frac{\pi}{2} - k_2\right]\Bigg\} \quad (-\pi \le \Delta\eta < \pi) \end{aligned} \tag{8}$$

where $k_1 = \sin^{-1}[\sqrt{r^2+\lambda^2}\cos(-\Delta\eta-\beta)]$ and $k_2 = \sin^{-1}(\sqrt{r^2+\lambda^2}\cos\beta)$. In (8), $\sqrt{r^2+\lambda^2}$ and $(\beta+\theta)$ are, respectively, the amplitude and phase of the complex-valued normalized correlation coefficient

$$\begin{aligned} r + \mathrm{i}\lambda &= \sqrt{r^2+\lambda^2}\cdot\exp[\mathrm{i}(\beta+\theta)] \\ &= \frac{\mathrm{E}(Y_1{}^* Y_2)}{\sqrt{\mathrm{E}(|Y_1|^2)\mathrm{E}(|Y_2|^2)}} \quad (-\pi \le \beta < \pi). \end{aligned} \tag{9}$$

Or, explicitly, r and λ can be computed as follows:

$$r = \frac{\mathrm{E}[\Re(Y_1)\cdot\Re(Y_2)]}{1/2\sqrt{\mathrm{E}(|Y_1|^2)\mathrm{E}(|Y_2|^2)}} = \frac{\mathrm{E}[\Im(Y_1)\cdot\Im(Y_2)]}{1/2\sqrt{\mathrm{E}(|Y_1|^2)\mathrm{E}(|Y_2|^2)}} \tag{10}$$

$$\lambda = \frac{\mathrm{E}[\Re(Y_1)\cdot\Im(Y_2)]}{1/2\sqrt{\mathrm{E}(|Y_1|^2)\mathrm{E}(|Y_2|^2)}} = -\frac{\mathrm{E}[\Im(Y_1)\cdot\Re(Y_2)]}{1/2\sqrt{\mathrm{E}(|Y_1|^2)\mathrm{E}(|Y_2|^2)}}. \tag{11}$$

Note that the expectation operations in (9)–(11) are also conditioned on the two transmitted signal vectors C_1 and C_2.

Adachi and Tjhung [7] considered the case in which the Rayleigh-faded signal vector $H \times C$ is uncorrelated with the additive Gaussian noise vector Z. However, (9) is a more general definition for the normalized correlation coefficient, $r + \mathrm{i}\lambda$, as it includes the case where the Rayleigh-faded signal vector and Gaussian noise vector are correlated. From (8), we can see that $(r + \mathrm{i}\lambda)$ *uniquely* determines the conditional cdf. In Fig. 3, we illustrate how the shape of the curve of the conditional cdf depends on the two parameters $\sqrt{r^2+\lambda^2}$ and β. The following two important observations can be made from Fig. 3.

A) The steepness of the curve of $\mathrm{G}(\Delta\eta|C_1, C_2)$ is determined by the amplitude of the normalized correlation coefficient, $\sqrt{r^2+\lambda^2}$. The closer to unity $\sqrt{r^2+\lambda^2}$ is, the steeper the curve. That is to say, the probability density function of $\Delta\eta$ approaches an ideal impulse as $\sqrt{r^2+\lambda^2}$ gets arbitrarily close to one.

B) At values of $\sqrt{r^2+\lambda^2}$ that are close enough to unity, the curve of $\mathrm{G}(\Delta\eta|C_1, C_2)$ approximates a staircase function and the sharp jump occurs at $\Delta\eta = -\beta$.

V. SER Performance Over Rayleigh Fading Channels

A. The Received OFDM Signal

From (2) and (4), the baseband received signal $u(t)$ at the output of the lowpass filter [point b in Fig. 1(a)], with additive Gaussian thermal noise taken into account, can be expressed as

$$u(t) = \sum_l h_l(t)s(t-\tau_l) + z_I(t) + \mathrm{i}z_Q(t) \tag{12}$$

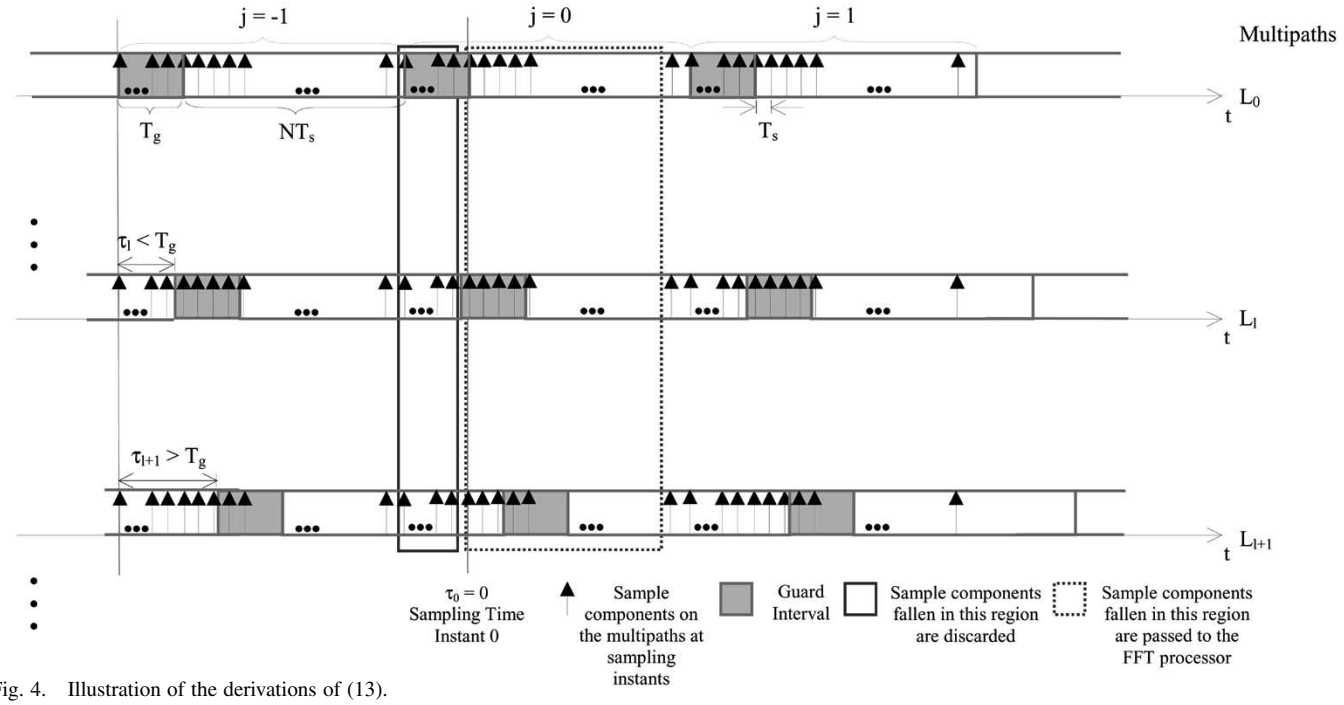

Fig. 4. Illustration of the derivations of (13).

where $z_I(t)$ and $z_Q(t)$ are zero-mean, bandlimited white Gaussian noise processes that are statistically independent of each other. The mean powers of $z_I(t)$ and $z_Q(t)$ are $\sigma^2_{z_I} = \sigma^2_{z_Q} = N_0/T_s$ [11].

Since perfect symbol synchronization is assumed, we can take $\tau_0 = 0$ in (12) and presume that the received waveform is sampled at time instants $\{nT_s\}$. Without loss of generality, the sample block $\{u(nT_s)|n = -N_g, \ldots, N-1\}$ corresponding to $j = 0$, as illustrated in Fig. 4, is investigated. We also assume that the largest delay $\tau_{L-1} < T$ so that each sample in this block can be written as

$$\begin{aligned} u(nT_s) = &\sum_{l\in \mathrm{R}_1(n)} h_l(nT_s)\sqrt{P_0}\sum_{k=0}^{N-1} C_{0,\mathrm{k}} \exp[\mathrm{i}\omega_0 k(nT_s - \tau_l)] \\ &+ \sum_{l\in \mathrm{R}_2(n)} h_l(nT_s)\sqrt{P_0} \\ &\cdot \sum_{k=0}^{N-1} C_{-1,\mathrm{k}} \exp[\mathrm{i}\omega_0 k(nT_s + T - \tau_l)] \\ &+ z_I(nT_s) + \mathrm{i}z_Q(nT_s) \quad n \in \{-N_g, \ldots, N-1\} \end{aligned} \tag{13}$$

where the two summation regions are defined as $\mathrm{R}_1(n) = \{l : 0 \le \tau_l \le T_g + nT_s\}$ and $\mathrm{R}_2(n) = \{l : \tau_l \ge T_g + nT_s\}$; the two regions are obtained by solving the inequality $N_g T_s \le nT_s - jT - \tau_l \le NT_s$ for a given $n \in \{0, 1, \ldots, N-1\}$ and a given $j \in \{-1, 0\}$. The derivation of (13) can be easily traced from Fig. 4.

The first N_g samples in this block are discarded, and the remaining N samples undergo the FFT process. The N post-FFT symbols can be written as

$$\begin{aligned} Y(m) &= \frac{1}{\sqrt{N}} \sum_{n=0}^{N-1} u(nT_s) \cdot \exp(-\mathrm{i}\omega_0 mnT_s) \\ &= H(m) \times C_{0,m} + \mathrm{ISI}(m) + \mathrm{ICI}(m) + N(m) \\ &\qquad (m = 0, 1, \ldots, N-1) \end{aligned} \tag{14}$$

where $H(m)$ represents the multiplicative fading effect

$$H(m) = \sqrt{\frac{P_0}{N}} \sum_{n=0}^{N-1} \sum_{l\in \mathrm{R}_1(n)} h_l(nT_s) \cdot \exp(-\mathrm{i}\omega_0 m\tau_l). \tag{15}$$

The ISI (m) contains symbols from previous block

$$\begin{aligned} \mathrm{ISI}(m) = &\sqrt{\frac{P_0}{N}} \sum_{n=0}^{N-1} \sum_{l\in \mathrm{R}_2(n)} h_l(nT_s) \\ &\times \sum_{k=0}^{N-1} C_{-1,k} \exp[\mathrm{i}\omega_0(k-m)nT_s] \\ &\times \exp[\mathrm{i}\omega_0 k(T - \tau_l)]. \end{aligned} \tag{16}$$

Notice that if all the multipath delays are smaller than the duration of the guard interval, the ISI will vanish. The intercarrier interference (ICI) (m) contributed by the other undesirable modulation symbols within the same block can be written as

$$\begin{aligned} \mathrm{ICI}(m) = &\sqrt{\frac{P_0}{N}} \sum_{n=0}^{N-1} \sum_{l\in \mathrm{R}_1(n)} h_l(nT_s) \sum_{\substack{k=0 \\ k\neq m}}^{N-1} C_{0,k} \\ &\exp[\mathrm{i}\omega_0(k-m)nT_s] \exp(-\mathrm{i}\omega_0 k\tau_l). \end{aligned} \tag{17}$$

Finally, $N(m)$, due only to the Gaussian thermal noise, can be written as

$$N(m) = \frac{1}{\sqrt{N}} \sum_{n=0}^{N-1} [z_I(n) + \mathrm{i}z_Q(n)] \exp(-\mathrm{i}\omega_0 mnT_s). \tag{18}$$

Note that the sequence $N(m)$ in (18) is statistically equivalent to the complex Gaussian noise $z_I(t) + \mathrm{i}z_Q(t)$ in (12).

B. Statistical Properties of the Fading, Interferences, and Noise

Since both the ISI (m) and the ICI (m) can be modeled as Gaussian noises due to the central limit theorem, it is easy to see that any adjacent FFT output symbols $Y(m-1)$ and $Y(m)$

in one block and the corresponding modulation symbols $C_{j,m-1}$ and $C_{j,m}$ can be represented by the phasor geometry in Fig. 2. Thus, the cdf of the differential phase angle in (8) can be used to obtain the SER formula. However, the normalized correlation coefficient, as defined in (9), has to be evaluated first.

In this paper, the data symbols $\{\theta_{j,k}\}$ are assumed to be equally probable. To evaluate the normalized correlation coefficient given in (9), we begin with the variance of $Y(m)$ given in (14). Let $F(m) = H(m) \times C_{0,m}$. It is easy to verify that $F(m)$, $\mathrm{ISI}(m), \mathrm{ICI}(m)$, and $N(m)$ are pairwise uncorrelated for any given m. Therefore, the variance of $Y(m)$ is the summation of the variances of $F(m), \mathrm{ISI}(m), \mathrm{ICI}(m)$, and $N(m)$. From (15)–(18), we can evaluate these variances to be in the following forms:

$$\begin{aligned}\sigma_F^2 &= \frac{1}{2}\mathrm{E}[F^*(m)\cdot F(m)\,|\,C_{0,m}] \\ &= \frac{P_0}{N}\sum_{n=0}^{N-1}\sum_{l\in \mathrm{R}_1(n)}\sigma_{h_l}^2 + \frac{2P_0}{N} \\ &\quad\times \sum_{n=1}^{N-1}\sum_{n'=0}^{n-1}\sum_{l\in \mathrm{R}_1(n')}\sigma_{h_l}^2\cdot \mathrm{J}_0(n-n') \qquad (19)\\ \sigma_{\mathrm{ISI}}^2 &= \frac{1}{2}\mathrm{E}[\mathrm{ISI}^*(m)\cdot \mathrm{ISI}(m)] \\ &= \frac{P_0}{N}\sum_{n=0}^{N-1}\sum_{l\in \mathrm{R}_2(n)}\sigma_{h_l}^2 \qquad (20)\\ \sigma_{\mathrm{ICI}}^2 &= \frac{1}{2}\mathrm{E}[\mathrm{ICI}^*(m)\cdot \mathrm{ICI}(m)] \\ &= \frac{P_0(N-1)}{N}\sum_{n=0}^{N-1}\sum_{l\in \mathrm{R}_1(n)}\sigma_{h_l}^2 \\ &\quad - \frac{2P_0}{N}\sum_{n=1}^{N-1}\sum_{n'=0}^{n-1}\sum_{l\in \mathrm{R}_1(n')}\sigma_{h_l}^2\cdot \mathrm{J}_0(n-n') \qquad (21)\\ \sigma_N^2 &= \frac{1}{2}\mathrm{E}[N^*(m)N(m)] = N_0/T_s \qquad (22)\end{aligned}$$

where $\mathrm{J}_0(n-n') = \mathrm{J}_0[2\pi f_D T_s(n-n')]$. It is interesting to note from the above expressions that all the variances are independent of the frequency index m. Thus, $\mathrm{E}[|Y(m)|^2] = \mathrm{E}[Y(m-1)|^2] = \sigma_F^2 + \sigma_{\mathrm{ISI}}^2 + \sigma_{\mathrm{ICI}}^2 + \sigma_N^2$. Now let us derive an expression for the correlation $\mathrm{E}[Y*(m-1)Y(m)]$. Denoting $I(m) = F(m) + \mathrm{ICI}(m)$, we can easily prove that $\{I(m)\}, \{\mathrm{ISI}(m)\}$, and $\{N(m)\}$, each as random vectors of size N, are uncorrelated with each other. Thus

$$\begin{aligned}&\frac{1}{2}\mathrm{E}[Y^*(m-1)\cdot Y(m)] \\ &\quad= \frac{1}{2}\mathrm{E}[I^*(m-1)I(m)] \\ &\qquad+ \frac{1}{2}\mathrm{E}[\mathrm{ISI}^*(m-1)\mathrm{ISI}(m)] \\ &\qquad+ \frac{1}{2}\mathrm{E}[N^*(m-1)N(m)]. \qquad (23)\end{aligned}$$

We now evaluate the correlations on the right-hand side of (23) as follows:

$$\frac{1}{2}\mathrm{E}[N^*(m-1)\cdot N(m)] = 0 \qquad (24)$$

$$\begin{aligned}&\frac{1}{2}\mathrm{E}[\mathrm{ISI}^*(m-1)\cdot \mathrm{ISI}(m)] \\ &\quad= P_0\sum_{n=0}^{N-1}\sum_{l\in \mathrm{R}_2(n)}\sigma_{h_l}^2\exp(-\mathrm{i}\omega_0 nT_s). \qquad (25)\end{aligned}$$

For the evaluation of the correlation between adjacent $I(m)$'s, we need to condition on the two modulation symbols $C_{0,m-1}$ and $C_{0,m}$; therefore

$$\begin{aligned}&\frac{1}{2}\mathrm{E}[I^*(m-1)\cdot I(m)\,|\,C_{0,m-1}, C_{0,m}] \\ &\quad= \exp(\mathrm{i}\theta_m)\frac{1}{2}\mathrm{E}\left[H^*(m-1)\cdot H(m)\right] \\ &\qquad+ \frac{1}{2}\mathrm{E}[\mathrm{ICI}^*(m-1)\cdot \mathrm{ICI}(m)] \qquad (26)\end{aligned}$$

where

$$\begin{aligned}&\frac{1}{2}\mathrm{E}[H^*(m-1)\cdot H(m)] \\ &\quad= \frac{P_0}{N}\sum_{n=0}^{N-1}\sum_{l\in \mathrm{R}_1(n)}\sigma_{h_l}^2\exp(-\mathrm{i}\omega_0\tau_l) \\ &\qquad+ \frac{2P_0}{N}\sum_{n=1}^{N-1}\sum_{n'=0}^{n-1}\sum_{l\in \mathrm{R}_1(n')}\sigma_{h_l}^2 \\ &\qquad\cdot \mathrm{J}_0(n-n')\cdot\exp(-\mathrm{i}\omega_0\tau_l) \qquad (27)\\ &\frac{1}{2}\mathrm{E}[\mathrm{ICI}^*(m-1)\cdot \mathrm{ICI}\,(m)] \\ &\quad= \frac{(N-2)P_0}{N}\sum_{n=0}^{N-1}\sum_{l\in \mathrm{R}_1(n)}\sigma_{\mathrm{h_l}}^2\exp(-\mathrm{i}\omega_0 nT_s) \\ &\qquad- \frac{2P_0}{N}\sum_{n=1}^{N-1}\sum_{n'=0}^{n-1}\sum_{l\in \mathrm{R}_1(n')}\sigma_{h_l}^2\cdot \mathrm{J}_0(n-n') \\ &\qquad\times[\exp(-\mathrm{i}\omega_0 nT_s) + \exp(-\mathrm{i}\omega_0 n'T_s)]. \qquad (28)\end{aligned}$$

Again, all the correlations are independent of m; therefore, for all the subcarriers, the normalized correlation coefficients are identical, and so are the cdfs of the differential angles. In the following, the SER performance of the OFDM system with MDPSK in frequency domain over Rayleigh fading channels with various delay and Doppler shift characteristics will be evaluated.

C. SER Performance Over Rayleigh Fading Channels

The decision regions for the MDPSK demodulation are $\{-\pi/M \le \Delta\eta \le \pi/M\}$. Since the data symbols $\{\theta_m\}$ are assumed to be equally probable, the SER is given by

$$\begin{aligned}P_s(\varepsilon) &= P_s(\varepsilon\,|\,\theta_m) \\ &= 1 - P\left(-\frac{\pi}{M}\le\Delta\eta\le\frac{\pi}{M}\right) \\ &= 1 - \left[\mathrm{G}\left(\frac{\pi}{M}\right) - \mathrm{G}\left(-\frac{\pi}{M}\right)\right] \qquad (29)\end{aligned}$$

where $\mathrm{G}(\cdot)$ is the conditional cdf defined in (8). From (29) and the fact that the function $\mathrm{G}(\cdot)$ is independent of m, we can see that the SERs on all subcarriers are identical for a given MDPSK

scheme. Since the cdf $\mathrm{G}(\cdot)$, is uniquely determined by the normalized correlation coefficient $r + \mathrm{i}\lambda$, we shall derive in this subsection the expressions for $r + \mathrm{i}\lambda$ that can be used to evaluate (8), and subsequently (29), for various types of Rayleigh fading channels.

1) Channels With $\tau_{L-1} < T_g, f_D T_s = 0$, and $\tau_{L-1} \ll NT_s$: Such channels are considered as frequency nonselective and slow fading (flat-flat fading) for our OFDM system, because, in this case, Y (m) is given by

$$Y(m) = F(m) + N(m) = H(m) \times C_{0,m} + N(m) \quad (30)$$

in which there is no ISI or ICI. From (19), (22)-(24), (26), and (27), we can show that for such channels

$$r + \mathrm{i}\lambda = \frac{e^{\mathrm{i}\theta_m}\mathrm{E}[H^*(m-1)H(m)] + \mathrm{E}[N^*(m-1)N(m)]}{\mathrm{E}[F^*(m)F(m)] + \mathrm{E}[N^*(m)N(m)]} = \frac{E_0}{E_0 + N_0}\exp(\mathrm{i}\theta_m). \quad (31)$$

In deriving the above expression, we have made the approximation that

$$\exp(-\mathrm{i}\omega_0\tau_l) \approx 1, \quad \text{for all } \tau_l. \quad (32)$$

This approximation is justified because $\tau_{L-1} \ll NT_s$ for such channels. If we define the energy per bit per subcarrier over one useful period as $E_b = E_0/\log_2 M$, and the bit energy to noise power density ratio as $\Gamma_\mathrm{b} = (E_b/N_0) \times (N + N_g)/N$, taking into consideration the energy loss due to the insertion of a guard interval, then (31) can be rewritten as

$$r + \mathrm{i}\lambda = \frac{1}{1 + 1\Big/\left(\Gamma_b \cdot \frac{N}{N+N_g} \cdot \log_2 M\right)}\exp(\mathrm{i}\theta_m). \quad (33)$$

Comparing (33) with (9), we have $\sqrt{r^2 + \lambda^2} = 1/\{1 + 1/[\Gamma_b \cdot N/(N + N_g) \cdot \log_2 M]\}$ and $\beta = 0$. From (33), we can see, in the flat-flat fading case, that both the amplitude and the phase β in the normalized correlation coefficient are independent of the particular power delay profile and the transmitted data symbols $\{\theta_m\}$. If the correlation between adjacent $Y(m)$'s is relatively high (say, $\sqrt{r^2 + \lambda^2} = 0.9$), the curve of the cdf will have a sharp jump around $\Delta\eta = 0$, which means a symbol error is most likely to occur in the adjacent decision regions of the correct one.

Since Gray mapping is used for the OFDM system, the bit-error rate (BER) can be approximated as $\mathrm{P_b}(\varepsilon) \approx \mathrm{P_s}(\varepsilon)/\log_2 M$. In Fig. 5, assuming $N/(N + N_g) = 85.80\%$, we plot BERs versus Γ_b for $M = 2, 4$, and 8 over flat-flat fading channels, together with the simulation result corresponding to OFDM-binary differential phase-shift keying (BDPSK) in frequency domain that is taken from [12, Fig. 6.16]. In the same figure, we also include three BER curves for OFDM-MDPSK ($M = 2, 4$, and 8) in time domain; among them, the one corresponding to BDPSK is taken from [13, Fig. 4], and the other two from [14, Fig. 4] with a slight modification to include

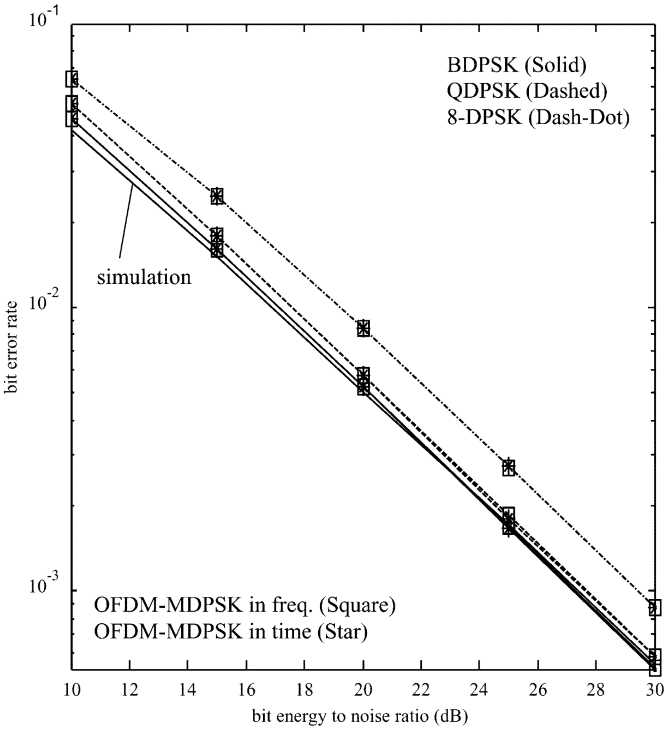

Fig. 5. BERs versus Γ_b for OFDM-BDPSK, -QDPSK, and -8DPSK in frequency/time domains over flat-flat Rayleigh fading channels.

a power penalty of $N/(N + N_g) = 85.80\%$. It can be seen from Fig. 5 that OFDM-MDPSK in frequency domain and its time domain counterpart have identical error-rate performance over flat-flat Rayleigh fading channels. In addition, the BER curve in Fig. 5 for OFDM-BDPSK in frequency domain agrees well with that for single-carrier BDPSK plotted in [11, Fig. 14-3-1] except for the power penalty. Theoretically speaking, for channels with $f_D T_s = 0$, i.e., time-nonselective channels, we can make them frequency nonselective to an OFDM system by selecting a sufficiently large guard interval that is greater than the largest multipath delay, and a very large value for N so that $\tau_{L-1} \ll NT_s$, and consequently, the transmission efficiency T_u/T, is high. The condition $\tau_{L-1} \ll NT_s$ implies that the channel coherence bandwidth is much larger than the bandwidth of each subchannel. Thus, a channel appearing frequency selective to a single-carrier system can be frequency nonselective to each individual OFDM subchannel (assuming both single-carrier and multicarrier systems support the same high data rate). Therefore, two adjacent OFDM subchannels will experience highly correlated fading, which makes the differential decoding and detection in the frequency domain desirable.

2) Channels With $\tau_{L-1} < T_g, f_D T_s = 0$, and τ_{L-1} a Significant Percentage of NT_s: The sampling period T_s is usually very small, as an OFDM system is designed for high data-rate transmission. Moreover, the total number of subcarriers N cannot be too large in practice, due to frequency offset and envelope variation problems [13]. Therefore, we may encounter cases where the maximum excess delay τ_{L-1} is a significant percentage of the useful period T_u. Such channels can be considered time dispersive, i.e., they appear frequency selective to each subcarrier. In this case, $Y(m)$ is still given by (30), but

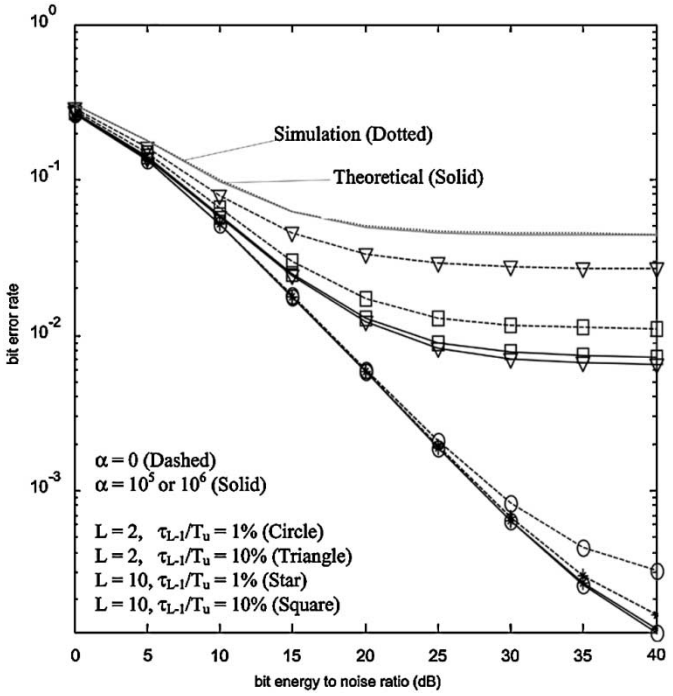

Fig. 6. BERs versus $\Gamma_{\rm b}$ for OFDM-BDPSK in frequency domain over time-dispersive Rayleigh fading channels.

the approximation in (32) is no longer valid. The normalized correlation coefficient now takes the following form:

$$r+\mathrm{i}\lambda=\frac{\exp(\mathrm{i}\theta_m)}{1+1/\left(\Gamma_b\cdot\frac{N}{N+N_g}\cdot\log_2 M\right)}\cdot\sum_{\text{all } l}\sigma_{h_l}^2\cdot\exp(-\mathrm{i}\omega_0\tau_l). \quad (34)$$

Notice from the above expression that, in the case of time-dispersive fading, both $\sqrt{r^2+\lambda^2}$ and β are still independent of the data symbols $\{\theta_m\}$, but they are now related to the normalized power delay profile and $\omega_0=2\pi/NT_s$.

In Fig. 6, we compare the theoretical BER computed using (8) and (29) with the simulation result of [12, Fig. 6.16] for OFDM-BDPSK in frequency domain. In plotting the theoretical BER curve of Fig. 6, we assume the same values for the system parameters as in [12], i.e., $\mathrm{N}=64, \tau_0=0, \tau_1/\mathrm{NT}_s=12.5\%, \mathrm{N}/(\mathrm{N}+\mathrm{N_g})=86.5\%, \alpha=0$, and $L=2$ (the last two parameters define a double spike profile with equal power). We can see that the theoretical and simulation results coincide. In Fig. 6, we also illustrate the effects of varying α and L on the BER for OFDM-BDPSK in the frequency domain. Here we assume that the delays are uniformly spaced between τ_0 and $\tau_{L-1}, N=256, T_s=1\ \mu$s, and power penalty $N/(N+N_g)=86.5\%$. However, we have adjusted the attenuation factor α from 10^6 at $\tau_{L-1}/NT_s=1\%$ to 10^5 at $\tau_{L-1}/NT_s=10\%$ for comparison purposes. This is to preserve the shapes (the relative strengths of the impulses) of power delay profiles having the same value of L when τ_{L-1} is varied. In comparing Fig. 6 with Fig. 5, we can immediately see that there are error floors in the case of time-dispersive fading. This can be explained as follows. In flat-flat fading, $\sqrt{r^2+\lambda^2}\to 1$ as $\Gamma_b\to\infty$ [see (33)], which means, in the limiting case, the cdf of the differential phase, $\mathrm{G}(\Delta\eta)$, will approach an ideal unit step function centered at the origin and there will be no detection error. In contrast, for time-dispersive fading, $\sqrt{r^2+\lambda^2}\to\left|\sum_{\text{all } l}\sigma_{h_l}^2\exp(-i2\pi\tau_l/NT_s)\right|$ as $\Gamma_b\to\infty$ [see (34)], which is less than unity. Therefore, the cdf in the limiting case will not be an ideal unit step function, and there will be a residual detection error. In Fig. 6, we can also observe that, if the shape of a delay profile is fixed, the larger τ_{L-1} is, or if we fix τ_{L-1} and L, the smaller the attenuation factor α is ($\alpha=0$ as compared with $\alpha=10^5/10^6$), the larger the BER will be at a specific $\Gamma_{\rm b}$. This is so because under both conditions, the channel root mean square (rms) delay spread increases, which implies the channel coherence bandwidth decreases, and therefore, the correlation between adjacent subchannels becomes smaller.

3) Channels With $\tau_{L-1}<T_g, f_DT_s\neq 0$, and $\tau_{L-1}\ll NT_s$: To ease the analysis without losing fundamental insight into the subject, we focus on the BDPSK scheme from this point onwards. In this part, the frequency-dispersive channel will be considered. The FFT output symbol $Y(m)$ is now given by

$$Y(m)=H(m)\times C_{0,m}+\mathrm{ICI}(m)+N(m). \quad (35)$$

Then, based on (19), (21)–(24), and (26)–(28), the normalized correlation coefficient is found to have the following form:

$$r+\mathrm{i}\lambda=\frac{\Lambda}{1+1/\left(\Gamma_b\cdot\frac{N}{N+N_g}\right)}\exp(\mathrm{i}\theta_m) \quad (36)$$

where

$$\Lambda=\frac{1}{N}+\frac{2}{N^2}\sum_{n=1}^{N-1}\sum_{n'=0}^{n-1}\mathrm{J}_0(n-n')-\frac{2\exp(-\mathrm{i}\theta_m)}{N^2}\sum_{n=0}^{N/N2}\sum_{n'=N/2}^{N-1}\mathrm{J}_0(n-n')\cdot[\exp(-\mathrm{i}\omega_0 nT_s)+\exp(-\mathrm{i}\omega_0 n'T_s)]. \quad (37)$$

In the above expressions, N is assumed to be an even integer. Comparing (36) with (9), we have $\sqrt{r^2+\lambda^2}=|\Lambda|/\{1+1/[\Gamma_b N/(N+N_g)]\}$ and $\beta=\arg(\Lambda)$. Neither $\sqrt{r^2+\lambda^2}$ nor β depends on channel power-delay profiles. However, both of them are functions of the total number of subcarriers N, the normalized maximum Doppler shift f_DT_s, and the data symbols $\{\theta_m\}$. The same comments can be made about the BER.

In Fig. 7, we compare our theoretical BERs with the simulation results of [12, Fig. 6.17] for OFDM-BDPSK in the frequency domain over frequency-dispersive channels, assuming $N=64, T_s=1\ \mu$s, double-spike profile with equal power, $f_DT_s=2.7\times10^{-4}$ (fast fading) or 1.35×10^{-5} (slow fading), $\{\theta_m\}=\{0,\pi\}$, and $N/(\mathrm{N}+\mathrm{N_g})=86.5\%$. The comparison shows that our theoretical BER curves agree quite well with the simulation results. As can be seen in the above figure, similar to the time-dispersive fading case, frequency-dispersive channels introduce error floors. The reason is the same as discussed in the previous part, i.e., $\sqrt{r^2+\lambda^2}\to|\Lambda|$, which is less than unity as

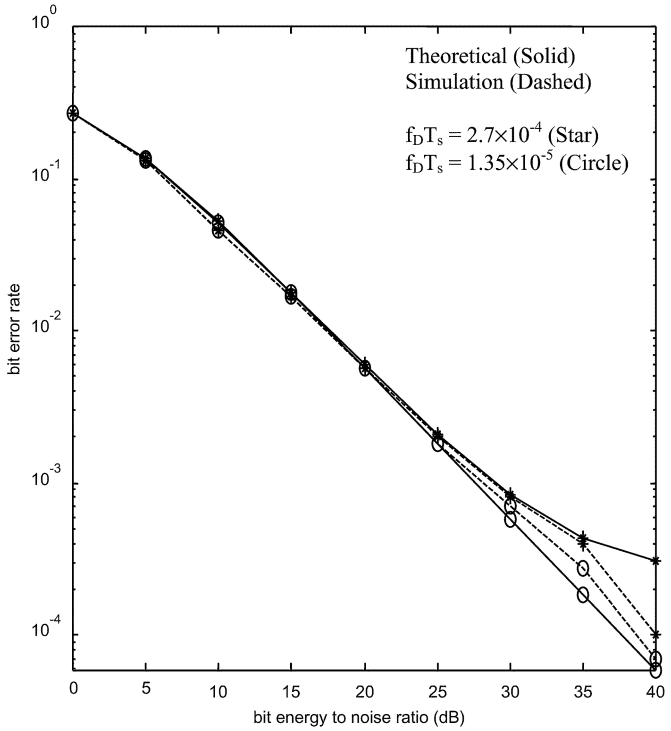

Fig. 7. Comparison of theoretical and simulated BERs versus Γ_b for OFDM-BDPSK in frequency domain over frequency-dispersive Rayleigh fading channels.

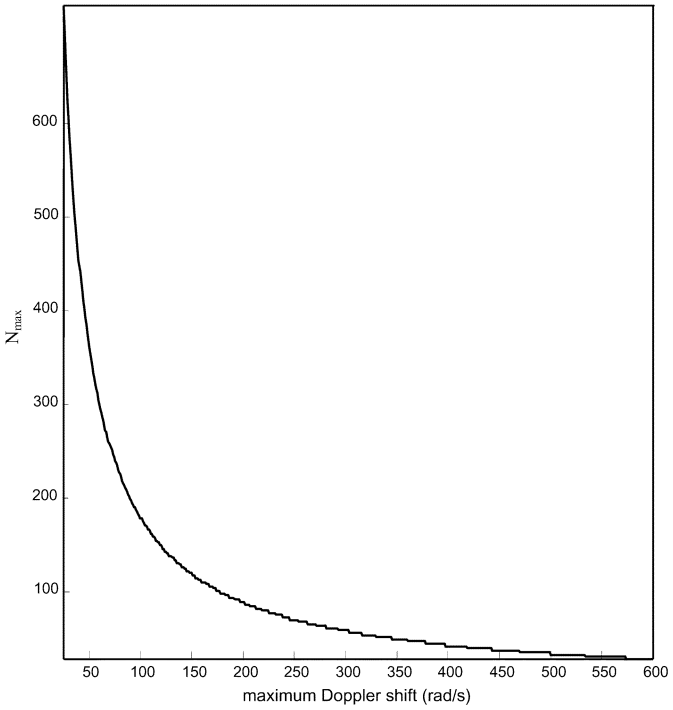

Fig. 8. $N_{\max}$ versus $2\pi f_D$ at the threshold of $|\Lambda| = 1 - 10^{-5}$.

$\Gamma_b \to \infty$. Obviously, the value of the error floor is a function of $N, f_DT_s, \{\theta_m\}$ and ω_0.

Abhishek [12, Fig 6.17] also compares the BER performance of both time- and frequency-domain OFDM-BDPSK systems over frequency-dispersive channels. It is revealed in [12] that both systems can achieve similar BER performance if the channel is slow fading, but OFDM-BDPSK in the frequency domain offers superior performance at large Γ_b (say, $\geq$10 dB) in a fast-fading environment. This is due to the reason that a rapid time variation of the channel has more destructive effect on the correlation of symbols on the same subcarrier in adjacent data blocks than on the correlation of symbols on adjacent subcarriers in the same data block.

4) Channels With $\tau_{L-1} < T_g$, $f_DT_s \neq 0$, and τ_{L-1} a Significant Percentage of NT_s: Such channels are considered doubly dispersive. For this type of channel, the FFT output symbol $Y(m)$ is still given by (35), but the normalized correlation coefficient takes the following form:

$$r + \mathrm{i}\lambda = \frac{\Lambda}{1 + 1/\left(\Gamma_b \cdot \frac{N}{N+N_g}\right)} \exp(\mathrm{i}\theta_m) \tag{38}$$

where

$$\Lambda = \frac{\nabla}{N} + \frac{2}{N^2} \sum_{n=1}^{N-1} \sum_{n'=0}^{n-1} \mathrm{J}_0(n-n')[\nabla - \exp(-\mathrm{i}\omega_0 nT_s - \mathrm{i}\theta_m) - \exp(-\mathrm{i}\omega_0 n'T_s - \mathrm{i}\theta_m)] \tag{39}$$

$$\nabla = \sum_{\text{all } l} \sigma_{h_l}^2 \exp(-\mathrm{i}\omega_0 \tau_l). \tag{40}$$

Unlike in the case of frequency-dispersive fading, now both $\sqrt{r^2+\lambda^2}$ and β, and therefore, the BER, explicitly depend on the channel power-delay profile and T_s, which is reflected by the parameter ∇ in (40).

5) Effect of Channel Characteristics on the Choice of T_s and N: As we have seen in parts C.2 and C.3 above, to minimize the time-dispersion effect of a channel with a given τ_{L-1}, the useful period T_u should be much longer than τ_{L-1}; whereas, to minimize the frequency-dispersion effect of a channel with a given f_D, the sampling period should be very small, such that $f_DT_s \ll 1$. However, these two requirements are often in conflict. To satisfy the delay requirement, either N or T_s or both should be large, but large N or T_s or both is undesirable for reducing the effect of ICI. Nevertheless, the conflict may not occur, at least in theory.

It can be concluded from the last two parts that, to achieve BER performance comparable to that achieved in the flat-flat fading case, the value of $|\Lambda|$ [see (37) and (39)] should be made as close to unity as possible. It can be graphically shown that, for a given nonzero f_DT_s, there exists a maximum value for N, exceeding which, the value of $|\Lambda|$ will fall below a certain threshold value (say, 1–10^{-4}), and consequently, the error floor will be raised above a certain level. Denote this maximum value as $N_{\max}$. In Fig. 8, we plot $N_{\max}$ versus $2\pi f_D$, assuming $T_s = 1$ μs and the channel is frequency dispersive only. The threshold value for $|\Lambda|$ is set at 1–10^{-5}, which corresponds to a bit-error floor of about 5×10^{-6}. The most important observation we can make from the figure is that $N_{\max}$ is exponentially increasing as f_DT_s decreases linearly. With this observation in mind, we can say that, theoretically, if there is no channel bandwidth constraint, then given arbitrary values of f_D and error floor, we can always find a small enough value for T_s such that $f_DT_s \ll 1$, but $N_{\max}T_s$ is so large as to make the

Rayleigh fading channel appear frequency nonselective to each subchannel.

6) Channels With $\tau_{L-1} > T_g$: In practice, the multipath spread may not be *a priori* known or it may change with time, so it is possible for the multipath spread to exceed the boundary of the guard interval. Therefore, it is of interest to envisage the SER/BER performance of the OFDM system over Rayleigh fading channels with $\tau_{L-1} > T_g$. In this part, we only consider the double-spike profile with equal power, in which $\tau_0 = 0$ and $\tau_1 = T_g + (n_1 - 1)T_s + \Delta t (1 \le n_1 \le N, 0 < \Delta t < T_s)$. Now, the FFT output symbol $Y(m)$ is given by the most general expression in (14). After some tedious algebra, the normalized correlation coefficient in this case is evaluated to be

$$r + \mathrm{i}\lambda = \frac{|\Lambda|}{1 + 1/[N\Gamma_b/(N+N_g)]} \exp[\mathrm{i}(\theta_m + \beta)] \qquad (41)$$

where

$$\begin{aligned}
&|\Lambda| \cdot e^{\mathrm{i}(\theta_m+\beta)} \\
&\quad = \frac{\exp(\mathrm{i}\theta_m)}{N}\left[\frac{\eta}{1+\eta} + \frac{(N-n_1)}{N(1+\eta)}\exp(-\mathrm{i}\omega_0\tau_1)\right. \\
&\qquad \left. + \frac{2\eta}{N(1+\eta)}\sum_{n=1}^{N-1}\sum_{n'=0}^{n-1}\mathrm{J}_0(n-n')\right] \\
&\qquad + \frac{2\cdot\exp[\mathrm{i}(-\omega_0\tau_1+\theta_m)]}{N^2(1+\eta)}\sum_{n=n_1+1}^{N-1}\sum_{n'=n_1}^{n-1}\mathrm{J}_0(n-n') \\
&\qquad - \frac{2}{N^2}\left[\frac{1}{(1+\eta)}\sum_{n=n_1}^{N-1}\exp(-\mathrm{i}\omega_0 nT_s)\right. \\
&\qquad + \frac{\eta}{(1+\eta)}\sum_{n=1}^{N-1}\sum_{n'=0}^{n-1}\mathrm{J}_0(n-n')\cdot\Psi \\
&\qquad \left. + \frac{1}{(1+\eta)}\sum_{n=n_1+1}^{N-1}\sum_{n'=n_1}^{n-1}\mathrm{J}_0(n-n')\cdot\Psi\right] \\
&\Psi = \exp(-\mathrm{i}\omega_0 nT_s) + \exp(-\mathrm{i}\omega_0 n'T_s). \qquad (42)
\end{aligned}$$

As can be seen from the above two equations, both $\sqrt{r^2+\lambda^2}$ and β, and therefore, the SERs/BERs depend on N, f_DT_s and $\{\theta_m\}$ for channels with $\tau_{L-1} > T_g$. In Fig. 9, we show the plots of BERs versus the rms delay spread at several values of Γ_b (power penalty: 0.67 dB) for OFDM-BDPSK in frequency domain over channels with double-spike profile of equal power. In the same figure, three BER curves corresponding to OFDM-BDPSK in time domain taken from [13, Fig. 6] are also included for comparison purposes. The same system parameter values as in [13] are used here, i.e., $T_u = 5.718\ \mu$s, $T_g = 952.4$ ns, $N = 8$, and $f_D = 0$. As can be seen from Fig. 9, for both time- and frequency-domain OFDM-BDPSK systems, there are sharp drops in BER when the second delay just exceeds the boundary of the guard interval. Furthermore, once the second delay exceeds the boundary of the guard interval, the BER curves at different Γ_b for either of the systems tend to merge, i.e., the ISI dominates error performance. Therefore, it is crucial to design a guard interval longer than all the multipath delays to avoid severe degradation of error-rate performance for both time- and frequency-domain OFDM-MDPSK systems.

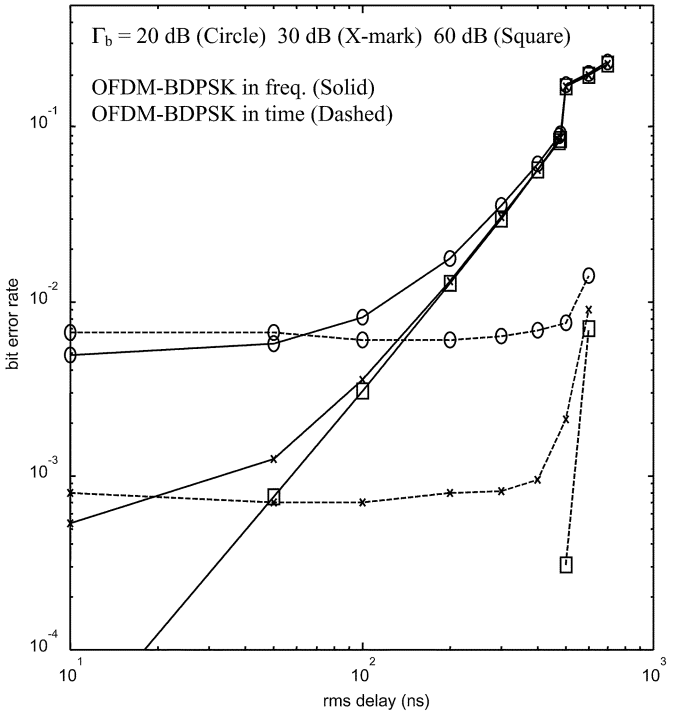

Fig. 9. BERs versus rms delay spread for OFDM-BDPSK in frequency/time domains over Rayleigh fading channels.

However, comparing the error-rate curves for OFDM-BDPSK in frequency domain and their time-domain counterparts in Fig. 9, we find that when the second delay is very small, the BERs achieved at $\Gamma_b = 20$ and 30 dB for both OFDM-BDPSK systems are nearly identical. As the second delay (therefore, the rms delay spread) increases, the BER for OFDM-BDPSK in frequency domain increases exponentially; while the BER for OFDM-BDPSK in time domain is relatively constant as long as the second delay does not exceed the length of the guard interval. That is to say, OFDM-MDPSK in frequency domain is less resilient to time-dispersion effects than its time-domain counterpart. The reason is that the correlation between adjacent subcarriers in one data block is smaller than that between symbols on one subcarrier in adjacent data blocks under pure time-dispersive channel conditions.

In Fig. 10, we show the plots of BERs versus normalized second delay (i.e., τ_1/T) at two values of f_DT_s (power penalty: 0.63 dB) for both time- and frequency-domain OFDM-BDPSK systems over channels with double-spike profile of equal power. The two curves for the time-domain system are taken from the simulation results of [12, Fig 6.15]. In plotting this figure, we assume that $T_g/T = 13.5\%$, $N = 64$, and $\Gamma_\mathrm{b} = 40$ dB. Again, we see that the time dispersion of channels has more destructive effect on frequency-domain OFDM-BDPSK systems than on its time-domain counterpart.

VI. Conclusion

We have applied Adachi and Tjhung's distribution function to obtain a closed-form formula for evaluating SER of the OFDM system with MDPSK in frequency domain over Rayleigh fading channels. We have found that identical SERs can be achieved on all the subcarriers for the system. However, both time and frequency dispersion of the channel will introduce error floors.

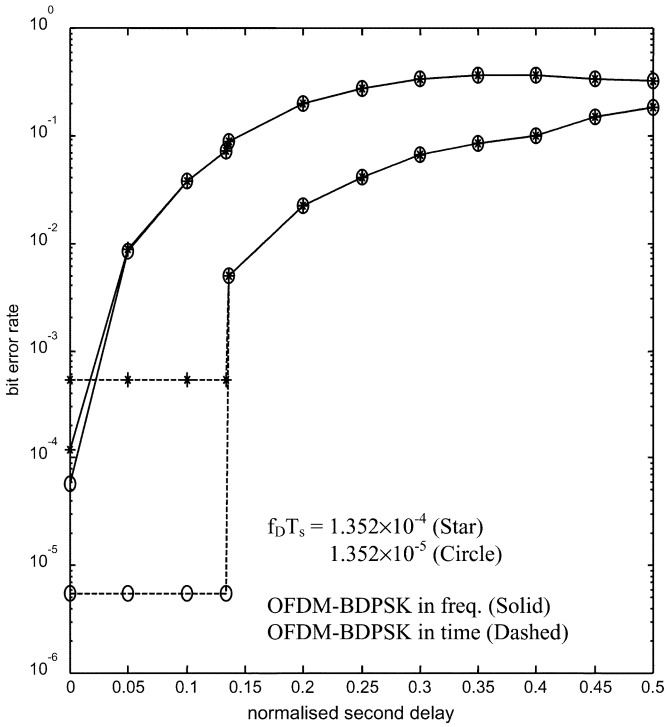

Fig. 10. BERs versus normalized second delay at two values of $f_D T_s$ for OFDM-BDPSK in frequency/time domains over Rayleigh fading channels.

We have also compared the error-rate performance and system model of OFDM-MDPSK in frequency domain and that in time domain. We have found that both systems give similar error-rate performance over flat-flat fading channels, but the former system offers superior performance over fast-fading channels, and the latter performs better in time-dispersive channels. Nevertheless, the error-rate performance of both systems will degrade significantly once the maximum multipath delay of the channel exceeds the boundary of guard interval. In addition, the former system is simpler to implement.

REFERENCES

[1] *European Standard (Telecommunications Series), Radio Broadcasting Systems; Digital Audio Broadcasting (DAB) to Mobile, Portable and Fixed Receivers*, ETSI EN 300 401 V1.3.3 (2001-05), 2001.

[2] *European Standard (Telecommunications Series), Digital Video Broadcasting (DVB); Framing Structure, Channel Coding and Modulation for Digital Terrestrial Television*, ETSI EN 300 744 V1.4.1 (2001-01), 2001.

[3] *Part 11: Wireless LAN Medium Access Control (MAC) and Physical Layer (PHY) Specifications*, IEEE 802.11a-1999, 1999.

[4] *Technical Specification, Broadband Radio Access Networks (BRAN); HIPERLAN Type 2; Physical (PHY) Layer*, ETSI TS 101 475 V1.2.2 (2001-02), 2001.

[5] *Technical Specification, Transmission and Multiplexing (TM); Access Transmission Systems on Metallic Access Cables; Asymmetric Digital Subscriber Line (ADSL)*, ETSI TS 101 388 V1.3.1 (2002-05), 2002.

[6] A. Dhir, "Wireless Home Networks: DECT, Bluetooth, HomeRF, and Wireless LANs," Xilinx, White Paper 135 (v1.0), Mar. 21, 2001.

[7] F. Adachi and T. T. Tjhung, "Distribution of phase angle between two Rayleigh vectors perturbed by Gaussian noise," *Inst. Elect. Eng. Electron. Lett.*, vol. 28, pp. 923–925, May 1992.

[8] W. C. Jakes, Jr., Ed., *Microwave Mobile Communications*. New York: Wiley, 1974, ch. 1.

[9] J. D. Parsons, *The Mobile Radio Propagation Channel*. London, U.K.: Pentech, 1992, ch. 5–6.

[10] L. Jun, T. T. Tjhung, F. Adachi, and L. Huang, "BER performance of OFDM-MDPSK system in frequency-selective Rician fading with diversity reception," *IEEE Trans. Veh. Technol.*, vol. 49, pp. 1216–1225, July 2000.

[11] J. G. Proakis, *Digital Communications*, 3rd ed. New York: McGraw-Hill, 1995, ch. 14.

[12] A. Oswal, "Effects of channel coding for OFDM/MDPSK system in Rayleigh fading channel," Master's thesis, Dept. Elect. Comput. Eng., Nat. Univ. Singapore, 2001.

[13] R. O'Neill and L. B. Lopes, "A study of novel OFDM transmission schemes for use in indoor environments," in *Proc. IEEE Vehicular Technology Conf.*, vol. 2, 1996, pp. 909–913.

[14] H. Ochiai and H. Imai, "MDPSK-OFDM with highly power-efficient block codes for frequency-selective fading channels," *IEEE Trans. Veh. Technol.*, vol. 49, pp. 74–82, Jan. 2000.

Kun Zhong was born in Chengdu, Sichuan, China, in December, 1976. He received the B.Eng. and M.Eng. degrees in electrical engineering from National University of Singapore, Singapore, in 2000 and 2001, respectively.

He is currently a Member of Technical Staff in the Centre for Communications Systems, DSO National Laboratories, Singapore, working in the area of design, analysis, and implementation of digital waveforms.

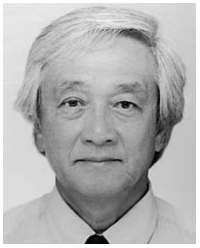

Tjeng Thiang Tjhung (SM'84) received the B.Eng. and M.Eng. degrees in electrical engineering from Carleton University, Ottawa, ON, Canada, in 1963 and 1965, respectively, and the Ph.D. degree from Queen's University, Kingston, ON, Canada in 1969.

From 1963 to 1968, he worked for Acres-Inter-Tel Ltd., Ottawa, ON, Canada, as a Consultant involved with the design of FSK systems for secure radio communication. In 1969, he joined the Department of Electrical Engineering, National University of Singapore, where he was appointed a Professor in 1985. He retired from the University in March 2001, and joined the Institute for Infocomm Research, Singapore, in April 2001 as a Principal Scientist. His present research interests are in, among others, multicarrier and code-division multiple-access (CDMA) techniques, and multiple-input multiple-output (MIMO) cum orthogonal frequency-division multiplexing (OFDM) communication systems.

Dr. Tjhung is a Member of the IEICE Japan and a Fellow of IES Singapore. He is also a Member of the Association of Professional Engineers of Singapore.

Fumiyuki Adachi (M'79–SM'90–F'00) received the B.S. and Dr. Eng. degrees in electrical engineering from Tohoku University, Sendai, Japan, in 1973 and 1984, respectively.

In 1973, he joined the Electrical Communications Laboratories of Nippon Telegraph & Telephone Corporation (now NTT) and conducted various types of research related to digital cellular mobile communications. From 1992 to 1999, he was with NTT Mobile Communications Network, Inc. (now NTT DoCoMo, Inc.), where he led a research group on wideband/broadband CDMA wireless access for IMT-2000 and beyond. From October 1984 to September 1985, he was a United Kingdom SERC Visiting Research Fellow in the Department of Electrical Engineering and Electronics at Liverpool University. From April 1997 to March 2000, he was a visiting Professor at Nara Institute of Science and Technology, Japan.Since January 2000, he has been with Tohoku University, Sendai, Japan, where he is a Professor of Electrical and Communication Engineering at the Graduate School of Engineering. His research interests are in CDMA and TDMA wireless access techniques, CDMA spreading code design, Rake receiver, transmit/receive antenna diversity, adaptive antenna array, bandwidth-efficient digital modulation, and channel coding, with particular application to broadband wireless communications systems.

Dr. Adachi served as a Guest Editor of IEEE JOURNAL OF SELECTED AREAS IN COMMUNICATIONS for a special issue on Broadband Wireless Techniques, October 1999, and for a special issue on Wideband CDMA I, August 2000, and Wideband CDMA II, January 2001. He was a corecipient of the IEEE TRANSACTIONS ON VEHICULAR TECHNOLOGY Best Paper of the Year Award in 1980 and again in 1990, and also a recipient of the Avant Garde award in 2000. He is a member of the Institute of Electronics, Information and Communication Engineers of Japan (IEICE) and was a recipient of the IEICE Achievement Award in 2002, and a corecipient of the IEICE Transactions Best Paper of the Year Award in 1996 and again in 1998.